Biophysical *Journal*
Article

Biophysical Society

Conformational Ensembles of Antibodies Determine Their Hydrophobicity

Franz Waibl,[1] Monica L. Fernández-Quintero,[1] Anna S. Kamenik,[1] Johannes Kraml,[1] Florian Hofer,[1] Hubert Kettenberger,[2] Guy Georges,[2] and Klaus R. Liedl[1,*]

[1]Department of General, Inorganic and Theoretical Chemistry, Center for Molecular Biosciences Innsbruck, University of Innsbruck, Innsbruck, Austria and [2]Roche Pharma Research and Early Development, Large Molecule Research, Roche Innovation Center Munich, Penzberg, Germany

ABSTRACT A major challenge in the development of antibody biotherapeutics is their tendency to aggregate. One root cause for aggregation is exposure of hydrophobic surface regions to the solvent. Many current techniques predict the relative aggregation propensity of antibodies via precalculated scales for the hydrophobicity or aggregation propensity of single amino acids. However, those scales cannot describe the nonadditive effects of a residue's surrounding on its hydrophobicity. Therefore, they are inherently limited in their ability to describe the impact of subtle differences in molecular structure on the overall hydrophobicity. Here, we introduce a physics-based approach to describe hydrophobicity in terms of the hydration free energy using grid inhomogeneous solvation theory (GIST). We apply this method to assess the effects of starting structures, conformational sampling, and protonation states on the hydrophobicity of antibodies. Our results reveal that high-quality starting structures, i.e., crystal structures, are crucial for the prediction of hydrophobicity and that conformational sampling can compensate errors introduced by the starting structure. On the other hand, sampling of protonation states only leads to good results when combined with high-quality structures, whereas it can even be detrimental otherwise. We conclude by pointing out that a single static homology model may not be adequate for predicting hydrophobicity.

SIGNIFICANCE Hydrophobicity is an important concept in the development of novel antibody-based therapeutics. Computational methods to evaluate hydrophobicity are typically based on hydrophobicity scales and either ignore the effects of the surroundings or model them through a sum of contributions of nearby residues. Here, we present a method based on molecular dynamics that does not include any per residue or per atom parameters except for the underlying force field and therefore automatically takes nonlinear effects into account in a physically meaningful way. We show that the method performs well at identifying hydrophobic antibodies if reliable structures are available and conclude that physics-based descriptors might lead to substantial improvements in computational assessment of hydrophobicity.

INTRODUCTION

In the past few decades, biopharmaceuticals have emerged as one of the largest areas of interest in the pharmaceutical industry. As of 2018, there were over 300 biopharmaceutical products licensed in the US, with the largest group of active agents being monoclonal antibodies (mAbs) (1–4). Though large improvements have been made in the discovery of mAbs binding to a certain target (5), problems may arise regarding the stability, solubility, or pharmacokinetics while developing an active mAb into a drug. Those properties are generally referred to by the term developability (6).

A major problem in the development process is the inherent tendency of some concentrated protein solutions to form aggregates. This problem may be influenced by various factors such as temperature, mechanical stress, and pH (7–9). Aggregation can be reversible or irreversible and covalent or noncovalent, and the resulting aggregates may be soluble or insoluble (8). Furthermore, multiple mechanisms of antibody aggregation have been discussed in literature (7,10), indicating that various factors contribute to antibody aggregation. Structural instability may lead to aggregation at both hot and cold temperatures (11,12), and hydrophobic surface patches have repeatedly been discussed to be involved (13,14) especially in the formation

Submitted June 18, 2020, and accepted for publication November 10, 2020.

*Correspondence: klaus.liedl@uibk.ac.at

Editor: Chris Chipot.

https://doi.org/10.1016/j.bpj.2020.11.010

of reversible aggregates (8). Furthermore, aggregation of antibodies should not be confused with amyloid aggregation, in which peptides or proteins form macroscopic, β-rich fibers or aggregates (15).

Hydrophobic patches on the surface of an antibody have been repeatedly discussed as one of the main contributions to aggregation propensity (8,16). Furthermore, hydrophobic patches can lead to high viscosity (17), though electrostatic properties are usually more predictive in this regard (17–19). Therefore, there is a strong interest in methods that can quantify the hydrophobicity of a biomolecule.

However, different definitions of hydrophobicity have been used in literature. The hydrophobicity of small molecules is usually quantified in terms of log p-values, which describe the ratio of the molecule's solubility in octanol and in water (20). In the field of secondary structure prediction, hydrophobicity scales are used to differentiate between amino acids in an aqueous environment and those in more hydrophobic regions such as membranes or in the protein's interior (21). The probability of a single amino acid to be buried in the hydrophobic core has been related to its free energy of solvation, ΔG_{solv} (22). Similarly, theoretical descriptions of hydrophobic interactions have focused on calculating ΔG_{solv} or related quantities (23).

The aim of this work is to explore whether hydrophobic molecules as identified by hydrophobic interaction chromatography (HIC) can also be distinguished from more hydrophilic ones via their free energy of solvation.

Experimental reference data

Several experimental methods have been devised to screen antibodies for their aggregation propensity during the early development stages. For instance, size-exclusion chromatography (24) is commonly used to determine the amount and the mass distribution of soluble aggregated species (25,26). Self-interaction chromatography (27) and cross-interaction chromatography (CIC) (28) measure the interactions of a protein with identical or similar protein molecules, respectively. Standup monolayer adsorption chromatography (SMAC) (29) measures the interaction of a protein with various side chains that resemble the polarity of protein surfaces. Affinity-capture self-interaction nanoparticle spectroscopy (AC-SINS) or salt-gradient AC-SINS quantify the interaction between antibodies bound to the surface of gold nanoparticles by measuring the phonon wavelength (30).

Hydrophobicity of antibodies is often quantified using HIC. This method measures the retention time of molecules in a hydrophobic column, whereas elution is achieved by gradually decreasing the salt concentration (31). There is a clear correlation between HIC retention times and phonon wavelengths from salt-gradient AC-SINS at comparable salt concentrations, which indicates that protein-protein interactions at such salt concentrations are dominated by the same forces as the interactions with a hydrophobic column (30). Furthermore, high HIC retention times of antibodies have been shown to correlate with increased nonspecific interactions with size-exclusion chromatography columns (31).

Throughout this study, we compare our computational results to a data set by Jain et al. (32). This data set contains 137 antibodies, for each of which 11 experimental assays have been performed. Because we attempt to quantify hydrophobicity rather than aggregation, we primarily focus on the hydrophobic HIC data. Furthermore, we use SMAC and CIC assay data. The main difference between those assays is that HIC quantifies interactions with a hydrophobic column, whereas SMAC uses a wide range of functional groups and CIC measures interactions with other (different) antibodies.

Computational estimation of hydrophobicity

The importance of hydrophobicity in antibody research is also highlighted by the number of tools that are aimed at aggregation prediction using hydrophobicity as a main parameter of their input data. For example, the spatial aggregation propensity (16) method is based on the hydrophobicity scale by Black and Mould (33). The therapeutic antibody profiler aims to detect antibodies with abnormal hydrophobic and electrostatic properties or loop lengths compared with clinical-stage antibodies (6). The AggScore algorithm uses descriptors for hydrophobic and electrostatic patches to detect aggregation-prone regions in antibodies (14).

Previous methods in the field of biomolecular research generally apply a residue-wise attribution of hydrophobicity or aggregation propensity based on predefined scales (34,35). Even though some methods contain contributions based on the three-dimensional protein structure, those contributions are generally not physics based. For instance, the spatial aggregation propensity algorithm applies an average of amino-acid-specific hydrophobicity values of nearby solvent-exposed residues (16), and the AggScore algorithm applies a Fermi-type function to weight the contribution of residues in the vicinity (14).

However, the strength of hydrophobic interactions in molecular systems is inherently nonadditive (36–38). Acharya et al. show a sigmoidal relationship between the perturbations in the hydration shell and the size of a hydrophobic patch (23). Furthermore, roughness can strengthen the effect of hydrophobic as well as hydrophilic surfaces (38). Therefore, we expect that any method based on a linear combination of hydrophobic contributions will not be able to fully describe the conformation dependence of protein hydrophobicity.

Many computational studies have been conducted that investigate the nature of hydrophobic interactions in detail. The interactions between water and a perfectly hydrophobic (i.e., noninteracting) particle can be physically described using the probability of randomly finding a cavity of the appropriate shape in bulk water (39,40). Other methods quantify hydrophobic interactions by simulating a mixture of water and multiple hydrophobic solutes and investigating the solute-solute radial distribution function (40). Those methods have proven effective in describing the hydration free energy of hydrophobic solutes of various sizes and at different temperatures. However, such studies have mostly been limited to simple systems such as noninteracting spheres (39), fully nonpolar molecules (39), or hydrophobic surfaces (23).

Here, we present an approach to describe the hydrophobicity of antibodies in terms of their hydration free energy, based on the GIST (grid inhomogeneous solvation theory) algorithm introduced by Nguyen et al. (41–44).

We have recently shown that GIST can directly estimate local hydrophobicity on the surface of a given protein based on its interactions with water molecules (45). We further introduced an enhanced GPU implementation of the GIST approach, in which we demonstrate a substantial increase of calculation speed. Thus, it is now possible to calculate hydration free energies, i.e., surface hydrophobicity, for large biomolecular systems such as serine proteases (45) or antibody fragments (this work) with high accuracy at manageable computational cost.

Sampling of conformations and protonation states

An additional challenge in predicting surface properties such as hydrophobicity lies in the inherently dynamic nature of antibodies. It has been well established that proteins constantly fluctuate between a multitude of conformational states (46,47). With these structural rearrangements, the local environment also changes, which can affect surface properties. Recent studies highlight their inherent flexibility of antibodies and its impact on physicochemical properties such as binding promiscuity or aggregation propensity (10,48–53). Molecular dynamics simulations offer the unique opportunity to capture this flexibility at atomic resolution (54). Current advances in the field, such as enhanced sampling techniques and Markov state modeling, allow for an efficient profiling of highly diverse structural ensembles (50–52).

In the interplay with conformational dynamics, there are several further environmental aspects contributing to surface hydrophobicity. As previously mentioned, one major determinant for the aggregation behavior of antibodies is the pH value. Small changes in pH can be enough to prevent or promote aggregation (8). The macroscopic change in pH is microscopically reflected by changes in the protein's protonation states. How and at which pH this reaction occurs is determined by the pK_a value of each titratable residue. However, the pK_a strongly depends on the local environment of a residue. Consequently, the pronation can change upon structural rearrangements, and variation of the protonation can further translate into altered local hydrophobicity.

However, a reliable prediction of protonation states is rather challenging. Multiple theoretical techniques have emerged to predict the pK_a values of a protein, either focusing on a static structure (e.g., PROPKA (55) or H++ (56)) or coupling the prediction with dynamics (family of constant pH methods (57,58)). It has been shown that constant pH molecular dynamics (CpHMD) simulations can closely reproduce experimental pK_a values while at the same time capturing pH-dependent structural changes of biomolecules (59).

Aim of this work

Here, we assess whether antibodies that exhibit high hydrophobicity in HIC experiments can be identified via their free energy of hydration as calculated from GIST. We combine state-of-the-art simulation techniques to investigate the distribution of hydrophobic regions on the surface of 126 Fv structures and compare the results with available experimental data from the literature (32). We employ Gaussian accelerated MD simulations (60) to capture diverse conformational ensembles. Furthermore, we incorporate the Monte-Carlo-based CpHMD framework to obtain protonation state ensembles. With the aid of our recent GPU-based implementation of the GIST algorithm (45), we are able to describe the hydrophobicity of antibodies while taking changes in structure and protonation into account.

METHODS

GIST

The hydrophobicity of a molecule is reflected by its interaction with water molecules. GIST (41–44,61) translates information on locations and orientations of water molecules into localized thermodynamic properties of water on a grid. This allows for an in-depth analysis of solvation around a solute, such as a protein in aqueous solution.

The GIST method provides information on the solvation free energy $\Delta G_{solv}(q_u)$ of a single solute conformation. In the case of a flexible solute, multiple GIST calculations of different solute conformations q_u must be performed. The overall ΔG_{solv} is then

$$\Delta G_{solv} = k_B T \ln \int p(q_u) e^{\frac{\Delta G^{solv}(q_u)}{k_B T}} dq_u, \qquad (1)$$

where k_B is Boltzmann's constant, T is the system temperature, and $p(q_u)$ is the probability of solute conformation q_u. A derivation of this equation is shown in the Supporting Materials and Methods. The following equations refer to a single conformation, but the parameter q_u will be omitted.

To calculate the individual $\Delta G_{solv}(q_u)$, the spatial integrals from the Inhomogeneous Solvation Theory (IST) are replaced by a discrete sum over voxels in a grid.

The localized, density-weighted free energy is split into energetic and entropic contributions (Eq. 2). The energy is again split into solvent-solvent and solute-solvent contributions (Eq. 3).

$$\Delta G(\boldsymbol{r}_k) = \Delta E_{total}(\boldsymbol{r}_k) - T\Delta S_{uv}^{total}(\boldsymbol{r}_k). \quad (2)$$

$$\Delta E_{total}(\boldsymbol{r}_k) = \Delta E_{vv}(\boldsymbol{r}_k) + \Delta E_{uv}(\boldsymbol{r}_k). \quad (3)$$

Here, G denotes the free energy, E the energetic contribution, T the temperature, and S the entropy; $\mathbf{r_k}$ are the coordinates of voxel k, u denotes the solute, and v denotes the solvent.

The entropy is approximated by the two-body solute-solvent entropy contribution, neglecting all higher order contributions. A comparison of the ΔG-, ΔE-, and ΔS-values to results from thermodynamic integration can be found in Loeffler et al. (62). They report good correlations between GIST and thermodynamic integration for the enthalpy and the free energy, whereas the entropy approximation is less accurate.

The solute-solvent term is further split into two different expressions for orientational and translational entropy (Eq. 4).

$$\Delta S_{uv}^{total}(\boldsymbol{r}_k) = \Delta S_{uv}^{trans}(\boldsymbol{r}_k) + \Delta S_{uv}^{orient}(\boldsymbol{r}_k). \quad (4)$$

Both the translational (ΔS^{trans}) and orientational (ΔS^{orient}) contributions to entropy are calculated using a nearest neighbor algorithm (Eqs. 5 and 6). Alternatively, both contributions can be computed together, approximating the six-dimensional integral over the rotational and orientational degrees of freedom (44).

$$S_k^{trans} = R\left(\gamma + \frac{1}{N_k}\sum_{i=1}^{N_k} \ln \frac{N_f \rho^0 4\pi \times d_{trans,i}^3}{3}\right). \quad (5)$$

$$S_k^{orient} = R\left(\gamma + \frac{1}{N_k}\sum_{i=1}^{N_k} \ln \frac{N_k (\Delta\omega_i)^3}{6\pi}\right). \quad (6)$$

$$S_k^{six} = R\left(\gamma + \frac{1}{N_k}\sum_{i=1}^{N_k} \ln \frac{N_f \rho^0 \pi \left(\Delta\omega_i^2 + d_{trans,i}^2\right)^3}{48}\right). \quad (7)$$

Here, R is the ideal gas constant, N_k is the total number of water molecules in voxel k, N_f is the total number of frames, γ is Euler's constant that corrects for an asymptotic bias, $d_{trans,i}$ is the cartesian distance between the solvent molecule i and its nearest neighbor, $\Delta\omega_i$ is the angular distance between solvent molecule i and its rotationally nearest neighbor in the same voxel, and ρ^0 is the number density of bulk solvent.

The interaction energy can readily be computed using the force field energy. Subsequent binning of the water molecules yields the solvent-solvent interaction energy E_{vv}, as well as the solute-solvent interaction energy E_{uv} in each voxel.

Starting structures

This work makes use of an experimental data set by Jain et al. (32). Two different subsets were defined: one set of 49 antibodies for which structures were available in the Protein Data Bank (PDB) (63), which will be called the "PDB set" hereafter. The accession codes we used can be found in Table S1.

Furthermore, a nonoverlapping set of 77 antibodies, for which no crystal structures were available, was investigated starting from homology models. The Rosetta antibody modeling protocol was used. To reduce the calculation time, the modeling was run partly on the ROSIE online server (64–68) and partly on the HPC infrastructure of the University of Innsbruck (LEO). For the local homology modeling calculations, we used Rosetta 2017.52 (68). We employed the kinematic loop closure (NGK) algorithm (69) to produce 1024 H3 loop models starting from the top grafted model, as well as 224 H3 loop models starting from the nine other (non-top-grafted) models, analogous to the ROSIE server. From each homology modeling run, the top-scored model was used as a starting structure. This set will be called the "homology models."

MD simulations

All simulations were performed using Amber18 (70). The ff14SB force field (71) was used for all simulations, together with the TIP3P (72) water model. Periodic boundary conditions were applied after solvating the systems in a cubic box with a minimal wall distance of 12 Å.

Simulations were performed using the PME algorithm (73) for long-range electrostatic interactions and a cutoff of 8.0 Å for the short-range interactions. A 2 fs time step was employed while constraining the length of all bonds involving hydrogen atoms using SHAKE (74). All simulations were performed in an NpT ensemble using the Langevin thermostat (75) at a temperature of 300 K and a collision frequency of 2 ps^{-1}, as well as a pressure of 1 bar. The Monte Carlo barostat (76) was employed with a volume change attempt every 100 steps for all simulations except the GIST calculations, for which a Berendsen barostat (77) was used with a pressure relaxation time of 1 ps.

Before starting production simulations, all starting structures were equilibrated following a protocol previously developed in our group (78).

Gaussian accelerated molecular dynamics (GaMD) simulations (60) were run applying a dual boost. The threshold energy was set to its upper limit. The number of simulation steps to update the potential energy statistics was set to four times the number of atoms in the system, according to the recommendation in the Amber manual (79), and rounded up to a multiple of 500. With a typical system size of 37,000 atoms and a 2 fs time step, this corresponds to ~300 ps. The closest multiple of this time to 2 ns was used as equilibration time, using conventional molecular dynamics. Similarly, the closest multiple of the averaging time to 6 ns was used to update the GaMD acceleration parameters. Subsequently, production simulations of 200 ns were performed using the final set of acceleration parameters.

CpHMD simulations were run in explicit solvent at a pH of 7.0 with a salt concentration of 0.1 mol/L (59). Protonation state changes were attempted every 200 steps, followed by 200 steps of solvent relaxation after a successful attempt. The production runs were 100 ns long.

Clustering and GIST analysis

GIST calculations were started for representative structures from a clustering of the respective simulations. Clustering was performed using the k-means algorithm (80) implemented in cpptraj (79) and in the case of GaMD simulations, cluster populations were reweighted using cumulant expansion to the second order (81). Five clusters were produced from each of the GaMD and CpHMD simulations. For each cluster representative, 20 ns of simulation were performed using a restraint weight of 1000 kcal $mol^{-1}Å^{-2}$ on all protein heavy atoms. 10,000 frames were collected. The center of mass of all Cα atoms was set to the origin. The GIST grid was also centered at the origin and sized in such a way that each atom is at least 7 Å away from the walls and that the number of voxels is a multiple of 10 in each direction, resulting in ~2×10^6 grid voxels. All analyses were performed using our recently published GPU implementation of the GIST algorithm (45).

Postprocessing

All postprocessing was performed using a set of in-house tools written in Python (81–83).

The protein structures were aligned to a reference using the ABangle core set as a selection mask (84). As reference, we used the Fv region of the PDB: 1N8Z structure, rotated in such a way that the x, y, and z axes correspond to the eigenvectors of the inertia matrix. The CDR loops point in the $+z$ direction and the heavy chain in the $+x$ direction. The coordinates of the GIST grids were transformed accordingly.

For all analyses, a reference value of −9.540 kcal/mol was subtracted from the normalized water-water interaction energy E_{vv}. This value was determined from a GIST calculation obtained from 100 ns cMD of a cubic water box containing 11,452 water molecules. 10,000 frames were used for the GIST analysis. The localized hydration free energy was calculated by summing up the water-water interaction energy, the solute-water interaction energy E_{uv}, and the entropy contribution calculated from a sixth-order integral $-T\Delta S^{six}$.

For further postprocessing, we first projected the free-energy contributions onto a set of predefined points on a unit sphere. To do so, we generated a set of 998 points using the method described by Deserno (85). We then selected all voxels within 5 Å of the protein, calculated their angular coordinates, and assigned each voxel to the closest sphere point based on the angular distance. We then summed the values of all voxels assigned to the same sphere point. We note that this procedure preserves the total hydration free energy, i.e., the sum over all sphere points is exactly the sum over all grid voxels.

The total ΔG_{solv} was calculated by summing the contributions of sphere points with $z > 0$, after applying a Gaussian blur with a sigma of 0.3 radians. By excluding points with z below 0, we omit the "lower" half of the Fv region, i.e., the one pointing toward the C_H2 domain. This is advantageous because the CDR loops, as well as their surroundings, are completely included, but the region that contacts the C_H2 domain is omitted. The latter would be problematic because omitting the C_H2 domain in the simulation can lead to artificial hydrophobic surfaces. Furthermore, we note that the Gaussian blur only alters the summed ΔG in the vicinity of the cutoff, effectively leading to a smooth cutoff in the z direction.

The spherical representation allows us to introduce a new metric, called $\Delta G_{unfavorable}$. For this metric, we apply a cutoff function that is zero below a cutoff ΔG_0 and linear above this cutoff (Eq. 8).

$$\Delta G_{unfavorable} = \begin{cases} \Delta G_{solv} - \Delta G_0 & \Delta G_{solv} > \Delta G_0 \\ 0 & \Delta G_{solv} \leq \Delta G_0 \end{cases}. \quad (8)$$

The constant ΔG_0 determines where the switching function transitions from zero to a linear function. Throughout this study, −0.2 was used. In contrast to the free energy of solvation, $\Delta G_{unfavorable}$ ignores the hydrophilic regions of an antibody while preserving all information about the most hydrophobic regions. Again, a total $\Delta G_{unfavorable}$ was calculated by summing all sphere points with $z > 0$. The performance of our method as a function of ΔG_0 is shown in Fig. 1 and the Supporting Materials and Methods.

Based on the spherical representation of $\Delta G_{unfavorable}$, we applied the uniform manifold approximation and projection (UMAP) (86) algorithm to project our GIST calculations onto a two-dimensional representation. UMAP is a dimension-reduction algorithm that is based on the assumption that the data are uniformly distributed on the Riemannian manifold and that tries to find a low-dimensional projection that preserves the local topological structure of the high-dimensional input data.

We applied a Gaussian blur to the spherical representation of our hydrophobicity data, using a standard deviation of 0.3 radians. We then apply UMAP using 30 points as the local neighborhood and a Euclidean distance metric. All parameters were kept at their default values.

For visualization purposes, we calculated the average contribution to the hydration free energy per water molecule in a shell of 5 Å around each atom and colored the protein surface according to those values for visualization purposes. The visualizations were done using PyMOL (87).

Reference data

We compare our computed ΔG_{solv}- and $\Delta G_{unfavorable}$-values to an experimental data set by Jain et al. (32). In this work, the results of 11 assays are presented for a set of 137 antibodies, all of which were either approved as drugs or undergoing clinical trials at the time of publication.

In our study, we primarily use the HIC retention time as a reference value for experimental hydrophobicity. Furthermore, we investigate the ability of our method to distinguish antibodies that strongly bind HIC, SMAC, or CIC columns from those that bind weakly to the same column.

A short summary of the experimental conditions that Jain et al. used for those assays (32) is given in the Supporting Materials and Methods.

RESULTS

Hydrophobicity computed from crystal structures and homology models

Following the procedure described in the Methods, we calculated solvation free energies ΔG_{solv}, as well as $\Delta G_{unfavorable}$, for 49 PDB structures and 77 homology models and compared the results to the experimental HIC retention times, as shown in Fig. 1, *A* and *D*. As explained in the Methods, we limit all our analyses to the upper half of the spherical projection, corresponding to the part of the antibody that is farthest away from the CH1-CL region and that contains the CDR loops.

The Pearson correlation between ΔG_{solv} and the HIC retention time is 0.43 for the PDB set and 0.17 for the homology models. The correlation between $\Delta G_{unfavorable}$ and the HIC retention time is 0.65 for the PDBs and 0.47 for the homology models. Using either metric, the results are significantly better using crystal structures than using homology models. Furthermore, the correlations using $\Delta G_{unfavorable}$ are significantly improved compared with those using ΔG_{solv}, which implies that HIC retention times are dominated by the most hydrophobic regions of an antibody.

Enhanced sampling using GaMD

To investigate the effect of conformational sampling on the accuracy of our method, we performed 200 ns GaMD simulations to obtain a structural ensemble. We used k-means clustering to obtain five representative structures of each trajectory and calculated ΔG_{solv} and $\Delta G_{unfavorable}$ as a weighted average using Eq. 1, as shown in Fig. 1, *B* and *E*. The error bars show the minimum and maximum of the values per cluster representative.

Using this approach, we obtain Pearson correlations of 0.45 and 0.26 between ΔG_{solv} and the HIC retention time for the PDB set and the homology models, respectively. The correlation between $\Delta G_{unfavorable}$ and the HIC retention time is 0.70 for the PDB set and 0.56 for the homology models.

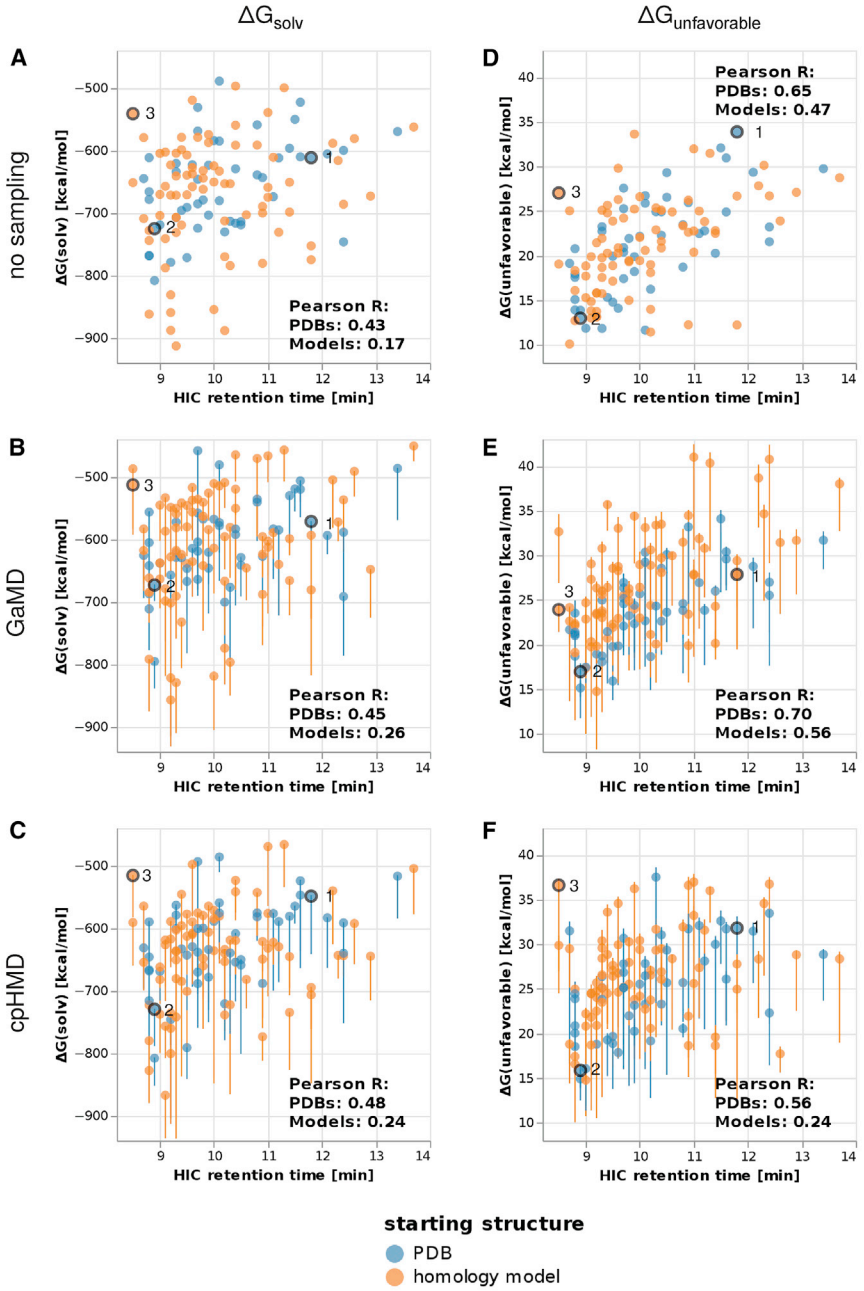

FIGURE 1 Total ΔG_{solv} (*A–C*) and $\Delta G_{unfavorable}$ (*D–F*), using different amounts of sampling. (*A* and *D*) No sampling. (*B* and *E*) 200 ns GaMD simulations. (*C* and *F*) 100 ns CpHMD. In the second and third row, each point represents the weighted average according to Eq. 1 of five GIST calculations started from different cluster representatives, and the error bars represent the minimum and maximum of the five individual values. Bevacizumab, muromonab, and dacetuzumab are labeled with 1, 2, and 3, respectively. To see this figure in color, go online.

As with the direct calculations, $\Delta G_{unfavorable}$ correlates significantly better with the HIC retention time than ΔG_{solv}. However, the conformational sampling only leads to a small improvement compared to the direct calculation. This is equally true for the PDB set and for the homology models, indicating that the sampling provided by GaMD is often insufficient to correct the errors introduced by the modeling. We note, however, that for some homology models that are predicted significantly too hydrophilic in Fig. 1 *D*, the conformational sampling provided by GaMD leads to significant improvements in the calculated $\Delta G_{unfavorable}$.

Protonation state sampling using CpHMD

Furthermore, we performed 100 ns CpHMD simulations to incorporate sampling of protonation states and calculated ΔG_{solv} and $\Delta G_{unfavorable}$ analogously, as shown in Fig. 1, *C* and *F*. We obtain Pearson correlations between ΔG_{solv} and the HIC retention time of 0.48 for the PDB set and of 0.24 for the homology models. The correlation between $\Delta G_{unfavorable}$ and the HIC retention time is 0.56 for the PDB set and 0.24 for the homology models.

Again, we find that $\Delta G_{unfavorable}$ performs significantly better than ΔG_{solv}. Furthermore, as with the structural

sampling, there is no large improvement compared to the direct GIST calculations. Interestingly, the correlation between $\Delta G_{unfavorable}$ and the HIC retention is even worse than without the protonation state sampling. This is less pronounced when (more reliable) PDB structures are used.

Combining conformational and protonation state sampling

To investigate the combined effect of structural sampling and protonation state sampling, we ran 10 ns CpHMD simulations starting from each of the cluster representatives of the GaMD simulations. We then fixed the protonation state of each amino acid to the most prominent state of the CpHMD and performed GIST calculations of those structures.

Fig. 2 shows the comparison of the calculated hydration free energies with the experimental HIC retention times. We find Pearson correlations of 0.52 and 0.67 using ΔG_{solv} and $\Delta G_{unfavorable}$, respectively. This is comparable to the results based directly on the representatives of the GaMD simulations, indicating that protonation states only play a minor role for hydrophobicity of antibodies.

Visualization of hydrophobicity

To set the obtained hydrophobicity estimates in a structural context, we projected the hydration free energy onto the protein surface. As an example, we show visualizations of three antibodies in Fig. 3. Bevacizumab and muromonab were chosen as hydrophobic and hydrophilic examples, respectively. Crystal structures of the Fab fragments are available in both cases. Furthermore, dacetuzumab was chosen as an example for which the hydrophobicity of the starting structure is overestimated based on a homology model but for which structural sampling leads to an improvement. The left column (Fig. 3, *A–C*) depicts the localized hydrophobicity of the three systems started from the most highly populated cluster of the ensemble captured with GaMD. It is clearly visible that there is a large hydrophobic region at the CDRs of bevacizumab, whereas muromonab is predicted to be significantly more hydrophilic. This is in line with experimental results, as reflected by the lower HIC retention time of muromonab (8.9 min) compared to bevacizumab (11.8 min).

When looking at the CpHMD representative of dacetuzumab, we find that there is a large cavity between the CDR-H3 and CRD-L3 loops. This leads to an increased surface hydrophobicity because residues of the hydrophobic core become solvent exposed. In the GaMD representative, this cavity has been closed, leading to a more realistic representation of dacetuzumab's hydrophobicity in solution.

Although the localized hydrophobicity in Fig. 3 facilitates visual comparison of different antibodies, this representation is not well suited for automated postprocessing workflows. We therefore seek to reduce the surface hydrophobicity data to a fixed number of points per antibody. To do so, we project ΔG_{solv} to points on the surface of a sphere, as described in the Methods. This projection is visualized in Fig. 4. In contrast to the depictions in Fig. 3, this representation is more suitable for postprocessing and might be used as input for machine learning or pattern recognition algorithms in future works.

Binary classification, receiver operating characteristic

To assess the capability of our method to detect antibodies that show increased hydrophobicity or other signs for nonspecific interactions, we separated the data set into delayed (retention time above the third quartile) and nondelayed (retention time $\leq$the third quartile) antibodies based on the HIC, SMAC, and CIC assays and plotted the receiver operating characteristic in Fig. 5, *A–C*, respectively. We generally find slightly better predictivity for HIC than for SMAC and CIC, with an AUC of 0.87 for the PDB set combined with GaMD sampling. In

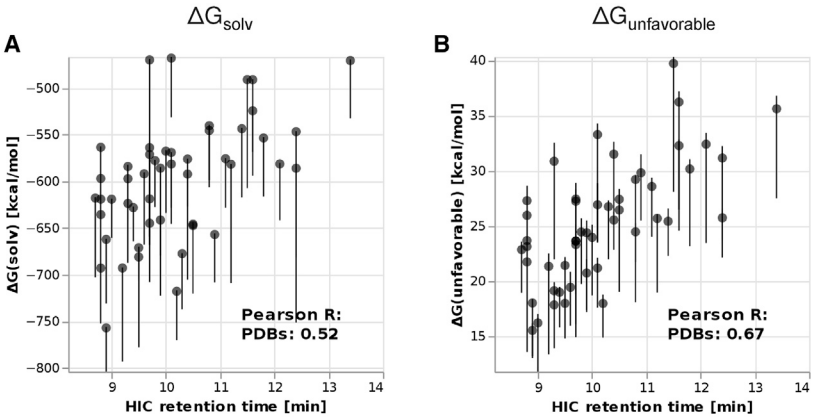

FIGURE 2 Total ΔG_{solv} (*A*) and $\Delta G_{unfavorable}$ (*B*) of the antibodies in the PDB set, using the combined structural and protonation sampling approach. Each point represents the weighted average according to Eq. 1 of five GIST calculations started from different cluster representatives, and the error bars represent the minimum and maximum of the same five values.

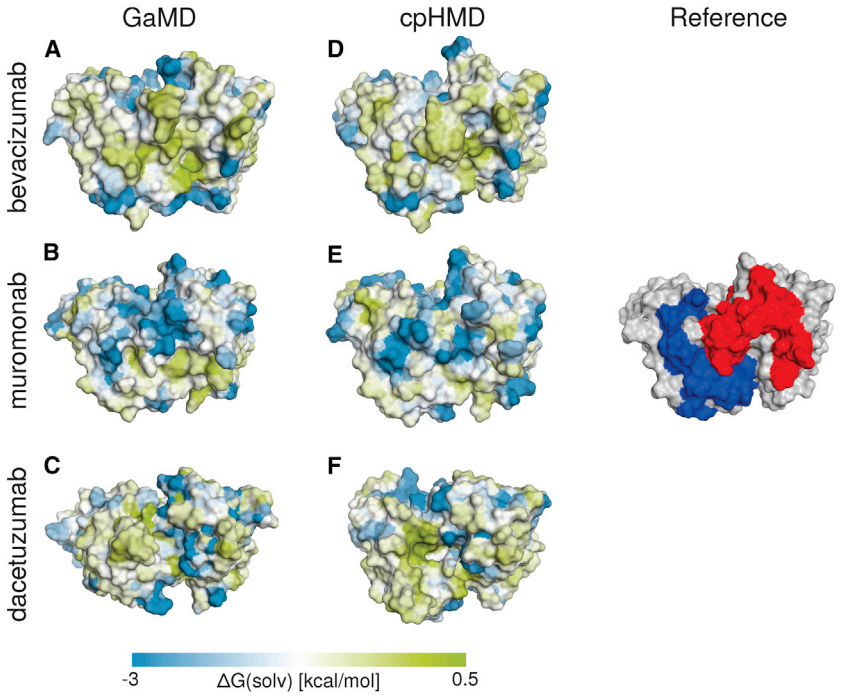

FIGURE 3 Averaged hydration free energy of the highest populated cluster representative mapped onto its surface representation using six different simulations. (*A* and *D*) Fv fragments of bevacizumab, (*B* and *E*) muromonab, and (*C* and *F*) dacetuzumab. (*A–C*) Cluster representatives from GaMD simulations. (*D* and *E*) Cluster representatives taken from CpHMD simulations. For reference, the surface of muromonab is also shown with the heavy chain CDR loops colored in red and the light chain CDR loops colored in blue, in the same orientation. To see this figure in color, go online.

accordance with the Pearson correlations shown in Fig. 1, the area under the curve (AUC) is significantly higher when starting from PDB structures as compared to homology models. An explanation could be that in both SMAC and CIC, interactions other than hydrophobic interactions, e.g., hydrogen bonding, may contribute to column retention.

Explorative data analysis using the UMAP algorithm

Because there is still a significant amount of unexplained variance when comparing the total hydration free energy to the experimental HIC data, we used the UMAP algorithm to create two-dimensional representations of our PDB and homology model sets. This algorithm aims at creating a low-dimensional representation of a data set while retaining the high-dimensional distance between similar points (86).

We compare the three different types of sampling (GaMD, CpHMD, or both) and the total ΔG_{solv} and $\Delta G_{unfavorable}$. The resulting plots are shown in Fig. 6.

DISCUSSION

In our study, we characterize the hydrophobicity of antibodies using GIST and investigate the impact of conformational diversity and pH on the predicted surface hydrophobicity. We compare our results with experimental HIC retention times from the literature. HIC has been shown to correlate with the aggregation behavior of antibodies (31), as well as with their aromatic amino acid content (88).

We investigate the impact of environmental effects like the pH or conformational diversity, which have been discussed in the literature as major contributors to surface hydrophobicity and aggregation propensity (89). It has been shown that the ability of an antibody to adopt various distinct conformations strongly influences its biophysical properties and function and thus dramatically increases the size of the antibody repertoire (90–94). This intrinsically flexible nature of antibodies and the crucial role of protonation render the prediction of surface properties difficult.

Various studies have shown that crystal packing effects can result in strong distortions of the CDR loops (53,95,96). These findings further emphasize that conformational sampling is vital to identify dominant structures in solution.

Our method is computationally slower than methods that rely on precalculated hydrophobicity scales, with several hundreds of nanoseconds of simulation time per antibody (with a typical system size around 37,000 atoms, we achieve simulation speeds around 200 ns/day on a GeForce GTX 2080 GPU; NVIDIA, Santa Clara, CA). However, the recent improvements to the GIST algorithm make it applicable to medium-sized data sets with around a hundred candidates. On the other hand, a big advantage of our method is that it does not make any prior assumptions on the relation between conformation and hydrophobicity and is thus well suited to investigate the impact of conformations or protonation states.

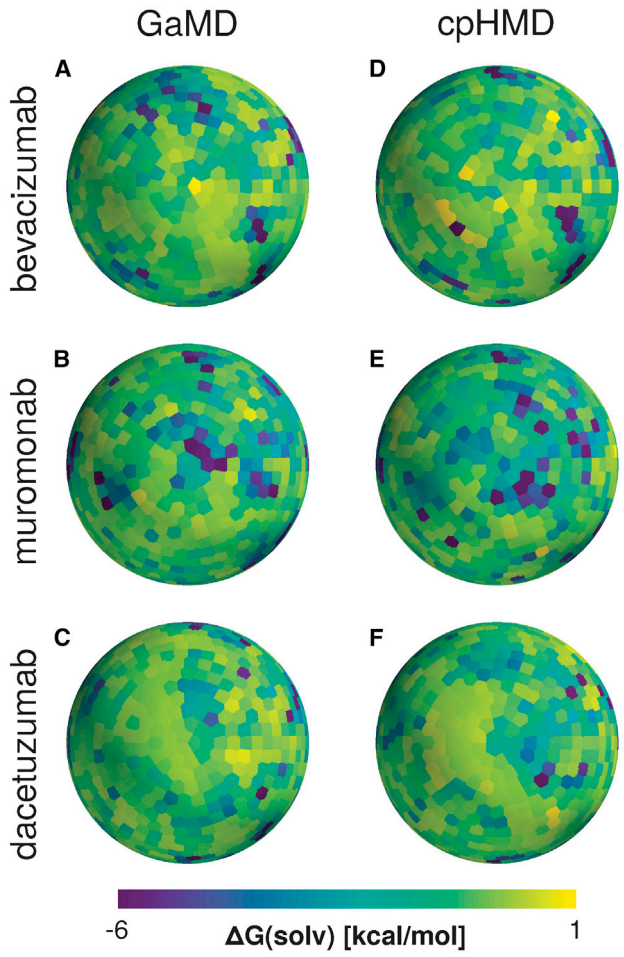

FIGURE 4 Spherical projections of the highest populated cluster representative of six different simulations. All spheres were generated after rotating the GIST grids according to the reference orientation shown in Fig. 3. (*A* and *D*) Fv fragments of bevacizumab, (*B* and *E*) muromonab, and (*C* and *F*) dacetuzumab. (*A–C*) Cluster representatives taken from GaMD simulations. (*D–F*) Cluster representatives taken from CpHMD simulations. The orientation of the spheres matches the surfaces in Fig. 3. To see this figure in color, go online.

Effects of the starting structure on hydrophobicity

Starting from a set of 49 crystal structures obtained from the PDB, as well as a set of 77 homology models of different antibodies, we perform GIST calculations to obtain the free energy of solvation ΔG_{solv}, as well as the free energy of hydrophobic regions $\Delta G_{unfavorable}$ as defined in Eq. 8. We compare our results with experimental HIC retention times and find significantly stronger correlations when using crystal structures than when using homology models. This shows that errors in the homology modeling procedure can have a large impact on the calculated surface hydrophobicity of antibodies.

Those findings emphasize the decisive role of reliable structures in the prediction of surface properties such as hydrophobicity. However, in the early stages of biopharmaceutical development, it is often not feasible to obtain crystal structures for each considered antibody. Therefore, substantial scientific efforts have been dedicated in recent years to improve structure prediction tools for antibodies (66–68,97).

The β-sheet framework of antibodies is structurally highly conserved and its structure prediction thus rather straightforward. However, accurate modeling of the CDR is less apparent. The CDR consists of six hypervariable loops known to strongly influence function and properties of an antibody (98). Five of these six CDR loops, except for the CDR-H3 loop, have been classified to a limited set of main-chain conformations, so-called canonical structures, according to their length and sequence (99–101). Therefore, their structure can be correctly predicted in many cases. However, structure prediction of the CDR-H3 loop remains challenging (97,101).

Our results show that potential shortcomings of the structure prediction strongly affect structure-based hydrophobicity predictions. This might be one reason for the continued popularity of sequence-based hydrophobicity prediction methods (13,102,103) because it implies that structure-based methods, which should, in principle, outperform their sequence-based counterparts, are significantly limited by the quality of their input structures.

Furthermore, we find that the distribution of ΔG_{solv} and $\Delta G_{unfavorable}$ is slightly different between PDB structures and homology models. On the one hand, some homology models have unusually low ΔG_{solv}-values, which can be seen most clearly in Fig. 1 *A*. Upon visual inspection, we found that many of those examples contain an accumulation of negatively charged residues. For instance, the L1 loop of lampalizumab contains four aspartate residues. It has been reported (104) that negatively charged residues have very negative hydration free energies in GIST calculations. Thus, we surmise that the conformation of such negatively charged residues strongly impacts the free energy of solvation ΔG_{solv}.

On the other hand, some homology models show an unusually high $\Delta G_{unfavorable}$, which can be seen best in Fig. 1 *E*. This metric focuses mainly on the most hydrophobic regions of an antibody while ignoring all details of the hydrophilic regions. Therefore, this implies that homology models are also not always optimal at burying hydrophobic side chains.

Effects of structural sampling on hydrophobicity

We performed GaMD simulations, which have been designed to capture an extended conformational space (60), on all of the 49 crystal structures and 77 homology models, and performed GIST calculations on five cluster representatives each.

Generally, we find that our simulations only lead to small improvements in the Pearson correlation between

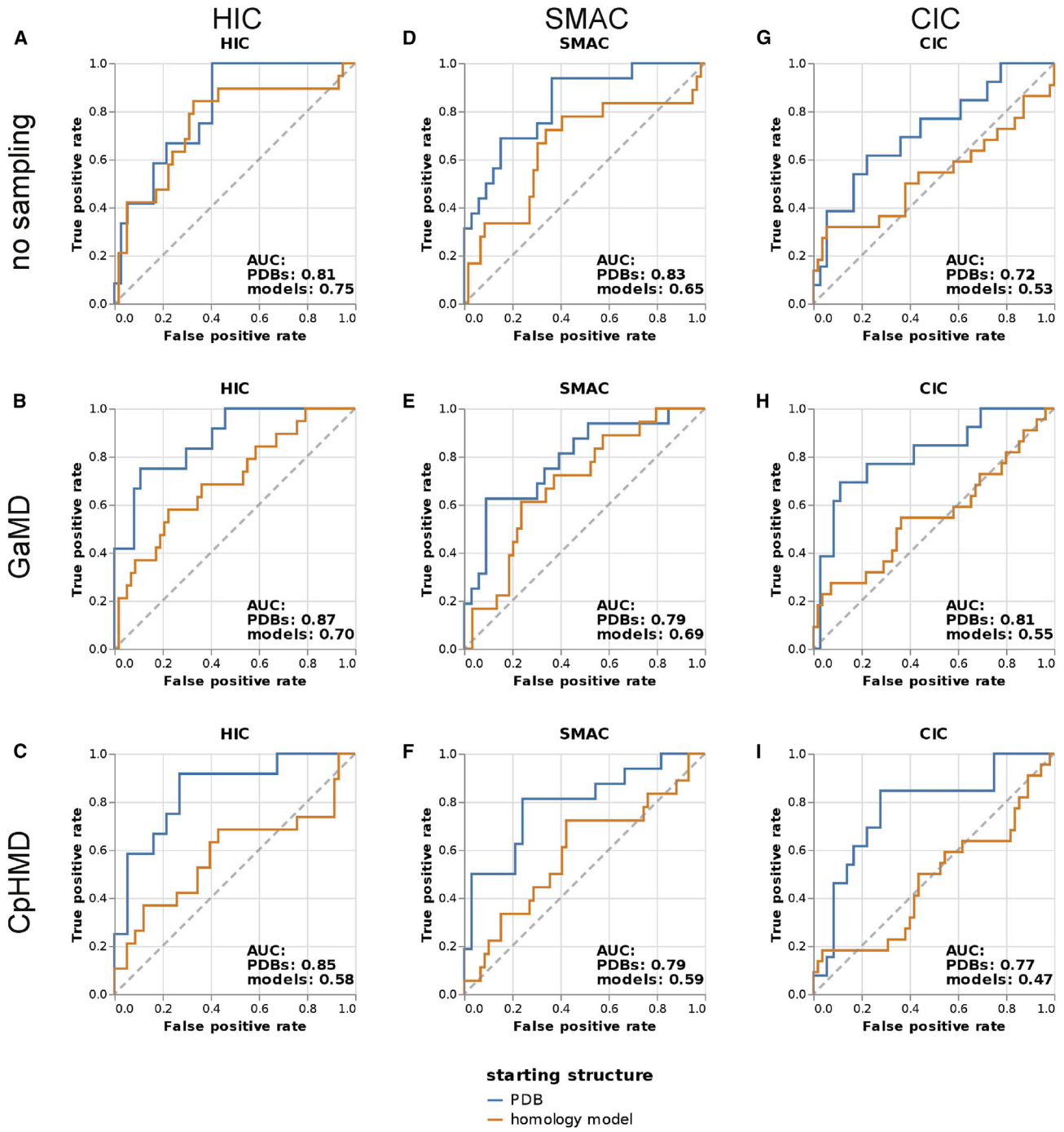

FIGURE 5 Receiver operating characteristic plots showing the ability of $\Delta G_{unfavorable}$ to separate between antibodies showing delayed (>3rd quartile) and normal (≤3rd quartile) elution based on the (*A–C*) HIC retention times, (*D–F*) SMAC retention times, and (*G–I*) CIC retention times. (*A*), (*D*), and (*G*) represent data collected without sampling, (*B*), (*E*), and (*H*) represent data from 200 ns GaMD simulation, and (*C*), (*F*), and (*I*) represent data from 100 ns CpHMD simulation. To see this figure in color, go online.

$\Delta G_{unfavorable}$ and experimental HIC retention times. This is true both for the crystal structures and for the homology models. For instance, we find a correlation of 0.65 when doing calculations on the PDB set without any sampling, which improves to 0.70 through the GaMD simulations. However, the considerable magnitude of the depicted error bars shows that there is strong variability of the surface hydrophobicity during the simulation. Together with the comparison between homology models and crystal structures, these findings show that protein conformation strongly impacts the hydrophobicity but that very long simulations might be necessary

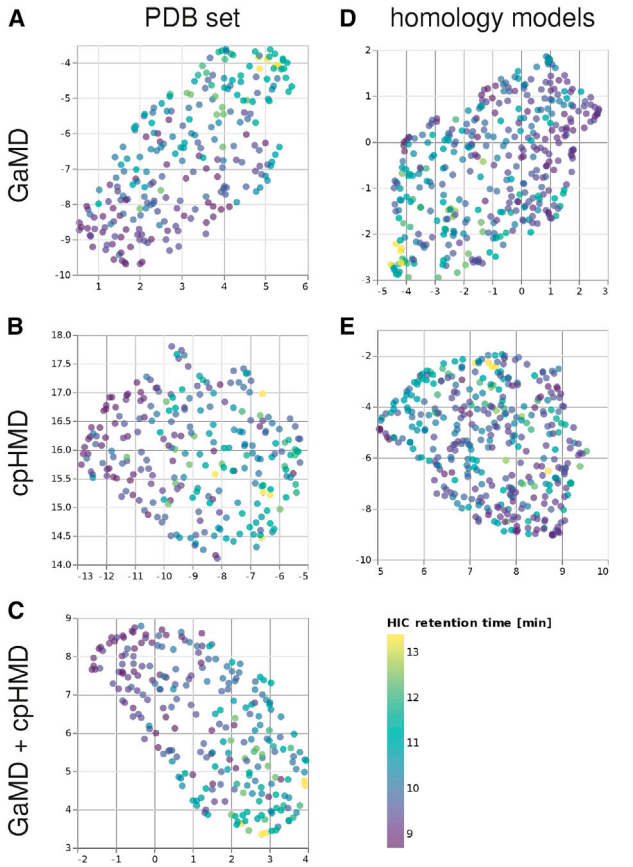

FIGURE 6 UMAP projections of the $\Delta G_{unfavorable}$ compared with the experimental HIC retention times. The five GIST simulations for each antibody are treated as individual data points. (*A–C*) PDB set. (*D* and *E*) Homology models. (*A* and *D*) Results using 200 ns of GaMD for sampling. (*B* and *E*) Results using 100 ns CpHMD. (*C*) Combined structural and protonation state sampling approach. To see this figure in color, go online.

to correct mistakes introduced during the homology modeling (50–52).

On the other hand, there are some cases of antibodies for which our simulations lead to significant improvements. Using $\Delta G_{unfavorable}$, there are some cases in which homology models are predicted significantly too hydrophilic without sampling (Fig. 1 *D*) and in which structural sampling using GaMD can improve the prediction (Fig. 1 *E*).

Furthermore, there are also examples where GaMD can correct an overprediction of hydrophobicity. For example, the experimentally hydrophilic antibody dacetuzumab displays high surface hydrophobicity both when using the homology model directly and when performing protonation state sampling with CpHMD, but not when using GaMD to cover a larger conformational space. This can be seen from the $\Delta G_{unfavorable}$-values in Fig. 1, *D–F*. Fig. 3, *C* and *F* visualize the localized free energy of solvation ΔG_{solv} of dacetuzumab in conformations from the CpHMD and GaMD ensembles, respectively. In the CpHMD structure, nonoptimal packing of side chains leads to exposure of hydrophobic residues from the VH-VL interface and therefore to an artificial hydrophobic patch on the surface. In the GaMD ensemble, however, this cavity is closed and the respective side chains are buried, leading to a more realistic estimation of the surface hydrophobicity.

Effects of protonation state sampling on hydrophobicity

Another factor of interest when calculating hydrophobicity and aggregation, besides the conformational ensemble, is the pH. Gentiluomo et al. have shown that even small changes in the pH can substantially shift the aggregation propensity (8). In contrast, our results show that protonation state sampling using CpHMD does not improve the prediction of HIC retention times and may even deteriorate the results when no reliable starting structures are available. This may be seen by comparing Fig. 1, *C* and *F* to Fig. 1, *A* and *D*.

Combining the protonation state sampling from CpHMD with starting structures from the PDB and the structural ensemble from GaMD, we again find better correlations to the HIC retention time, which are comparable with the results using GaMD only.

Taken together, these findings indicate that protonation states are not the primary source of error in our hydrophobicity calculations. On the other hand, the abovementioned study by Gentiluomo et al. (8) found a strong influence of the pH on aggregation. However, we note that hydrophobicity and aggregation propensity are different properties. It is plausible that interactions of a protein with a hydrophobic column are less charge dependent than protein-protein interactions.

Total ΔG vs. ΔG of hydrophobic regions

In Fig. 1, we compare both the total hydration free energy ΔG_{solv} and the hydrophobic free energy $\Delta G_{unfavorable}$ to experimental HIC retention times and find significantly better Pearson correlations using $\Delta G_{unfavorable}$. The difference between those metrics is that $\Delta G_{unfavorable}$ only takes the most hydrophobic surface regions into account, whereas ΔG_{solv} describes the solvent-water interaction of the whole molecule. This indicates that the interaction between antibodies and HIC columns is dominated by the most hydrophobic regions of the antibody surface. Similar ideas have been proposed in the literature (105). Furthermore, our result is consistent with the common practice to base hydrophobicity predictions on quantities like the areas of hydrophobic patches (105), which also disregards the more hydrophilic surface regions.

UMAP

To show how our spherical projection might be used as input for further data analysis, we project our data set to a two-dimensional subspace using the UMAP method. The results

are shown in Fig. 6. Consistent with our previous analyses, we find a clearly better separation of high and low HIC retention times in the PDB set than in the homology models, which further indicates that characterization of surface hydrophobicity strongly depends on the initial structure. Furthermore, we observe that protonation state sampling using CpHMD leads to very poor separation when applied to homology models, whereas the results are quite good when crystal structures or, even better, a combination of crystal structures and conformational sampling is available as the structural basis for the CpHMD. Hence, as discussed above, the impact of conformational sampling clearly outweighs solely optimizing the protonation states.

A main difference between the UMAP results depicted in Fig. 6 and the preceding analysis is that the latter show ensemble averages. In the UMAP projections, on the other hand, each of the five cluster representatives per antibody is depicted individually. The UMAP algorithm can clearly identify cluster representatives that belong to the same antibody, whereas a simple summation of ΔG_{solv} or $\Delta G_{unfavorable}$ leads to very high noise because of conformational differences.

Our hypothesis is that the summed ΔG-values suffer more from the noise that is introduced by taking a limited set of structures from the conformational ensemble. Because solvation is conformation dependent, antibodies can have different ΔG_{solv} and $\Delta G_{unfavorable}$ even in regions that are identical in their sequence, because of the limited sampling of conformations. In the UMAP calculations, a Euclidean distance metric is used that automatically places higher weights on strongly different regions, thus favoring real structural differences over random deviations from the limited sampling. The good separation in Fig. 6 *C* indicates that this is a better use of the available information and that this translates to reduced two-dimensional space. However, further work will need to be done to see how this can be used to improve hydrophobicity predictions.

Binary classification and receiver operating characteristic

We test the performance of our method in performing a binary classification, i.e., in detecting the most hydrophobic antibodies of our data set. We find an AUC of 0.87 for the detection of delayed elution in a HIC column and an AUC of 0.79 when comparing to a SMAC column (using the GaMD results). This shows that our method can be useful in filtering the strongest-binding antibodies from a data set, even though not all antibodies are predicted correctly. However, we again observe that the predictivity of our method substantially deteriorates when using homology models instead of PDB structures, indicating that high-quality structures are necessary to detect hydrophobic antibodies based on protein-water interactions.

CONCLUSIONS

We have developed a purely physics-based method to predict the hydrophobic behavior of antibodies based on a localized description of the free energy of hydration. Our method does not contain any residue-specific hydrophobicity parameters but performs well at predicting the relative aggregation propensity in a set of antibodies, especially when reliable structural information is available. Furthermore, our method allows a visualization of the hydrophobicity on the antibody surface, which might be a valuable tool for rational design of less aggregation-prone antibody variants.

Our analyses show that high a quality structure is crucial for the correct prediction of surface hydrophobicity using physics-based methods. The correlation between our metrics and experimental hydrophobicity is significantly better when using crystal structures than when using homology models as starting structure. Furthermore, we highlight that conformational sampling, i.e., describing hydrophobicity as an ensemble property, can reduce inaccuracies resulting from the uncertainties of structure prediction tools. However, we also show that structural inaccuracies can be long lived in molecular dynamics simulations, which represents a major challenge for structure-based hydrophobicity prediction, especially when large data sets are investigated.

Our results show that hydrophobicity is strongly dependent on the protein conformation. Ensembles generated from homology models may overestimate hydrophobicity, indicating that those structures are unable to sufficiently bury their hydrophobic side chains. We also investigate the effect of protonation state sampling on hydrophobicity and find that it only performs well when combined with enhanced sampling techniques because the protonation states are themselves conformation dependent.

Furthermore, we show that localized data on the hydration free energy can be used as input for the UMAP dimensionality reduction method. We presume that the localized information that our method provides will enable substantial improvements to our prediction quality once we gain a deeper understanding of the postprocessing methodology.

SUPPORTING MATERIAL

Supporting Material can be found online at https://doi.org/10.1016/j.bpj.2020.11.010.

AUTHOR CONTRIBUTIONS

F.W. performed research and wrote most of the manuscript. M.L.F.-Q. performed research. A.S.K. analyzed data. J.K. assisted with the GIST calculations. F.H. assisted with the CpHMD simulations. H.K. helped supervising the research. G.G. helped supervise the research. K.R.L. supervised the research. All authors contributed to writing the manuscript.

ACKNOWLEDGMENTS

The computational results presented her have been achieved (in part) using the LEO HPC infrastructure of the University of Innsbruck.

This work was supported by the Austrian Science Fund via the grants P30565, P30737, and P30402, as well as DOC 30. H.K. and G.G. are Roche employees. Roche has an interest in developing antibody-based therapeutics.

REFERENCES

1. Walsh, G. 2018. Biopharmaceutical benchmarks 2018. *Nat. Biotechnol.* 36:1136–1145.
2. Kaplon, H., and J. M. Reichert. 2018. Antibodies to watch in 2018. *MAbs.* 10:183–203.
3. Kaplon, H., M. Muralidharan, …, J. M. Reichert. 2020. Antibodies to watch in 2020. *MAbs.* 12:1703531.
4. Kaplon, H., and J. M. Reichert. 2019. Antibodies to watch in 2019. *MAbs.* 11:219–238.
5. Mould, D. R., and B. Meibohm. 2016. Drug development of therapeutic monoclonal antibodies. *BioDrugs.* 30:275–293.
6. Raybould, M. I. J., C. Marks, …, C. M. Deane. 2019. Five computational developability guidelines for therapeutic antibody profiling. *Proc. Natl. Acad. Sci. USA.* 116:4025–4030.
7. Mahler, H. C., W. Friess, …, S. Kiese. 2009. Protein aggregation: pathways, induction factors and analysis. *J. Pharm. Sci.* 98:2909–2934.
8. Gentiluomo, L., D. Roessner, …, W. Frieß. 2020. Characterization of native reversible self-association of a monoclonal antibody mediated by Fab-Fab interaction. *J. Pharm. Sci.* 109:443–451.
9. Hauptmann, A., G. Hoelzl, and T. Loerting. 2019. Distribution of protein content and number of aggregates in monoclonal antibody formulation after large-scale freezing. *AAPS PharmSciTech.* 20:72.
10. Codina, N., D. Hilton, …, P. A. Dalby. 2019. An expanded conformation of an antibody Fab region by X-ray scattering, molecular dynamics, and smFRET identifies an aggregation mechanism. *J. Mol. Biol.* 431:1409–1425.
11. Lazar, K. L., T. W. Patapoff, and V. K. Sharma. 2010. Cold denaturation of monoclonal antibodies. *MAbs.* 2:42–52.
12. King, A. C., M. Woods, …, M. R. H. Krebs. 2011. High-throughput measurement, correlation analysis, and machine-learning predictions for pH and thermal stabilities of Pfizer-generated antibodies. *Protein Sci.* 20:1546–1557.
13. Conchillo-Solé, O., N. S. de Groot, …, S. Ventura. 2007. AGGRESCAN: a server for the prediction and evaluation of "hot spots" of aggregation in polypeptides. *BMC Bioinformatics.* 8:65.
14. Sankar, K., S. R. Krystek, Jr., …, J. K. X. Maier. 2018. AggScore: prediction of aggregation-prone regions in proteins based on the distribution of surface patches. *Proteins.* 86:1147–1156.
15. Rousseau, F., J. Schymkowitz, and L. Serrano. 2006. Protein aggregation and amyloidosis: confusion of the kinds? *Curr. Opin. Struct. Biol.* 16:118–126.
16. Voynov, V., N. Chennamsetty, …, B. L. Trout. 2009. Predictive tools for stabilization of therapeutic proteins. *MAbs.* 1:580–582.
17. Nichols, P., L. Li, …, M. J. Allen. 2015. Rational design of viscosity reducing mutants of a monoclonal antibody: hydrophobic versus electrostatic inter-molecular interactions. *MAbs.* 7:212–230.
18. Agrawal, N. J., B. Helk, …, B. L. Trout. 2016. Computational tool for the early screening of monoclonal antibodies for their viscosities. *MAbs.* 8:43–48.
19. Tomar, D. S., L. Li, …, S. Kumar. 2017. In-silico prediction of concentration-dependent viscosity curves for monoclonal antibody solutions. *MAbs.* 9:476–489.
20. Low, Y. W., F. Blasco, and P. Vachaspati. 2016. Optimised method to estimate octanol water distribution coefficient (logD) in a high throughput format. *Eur. J. Pharm. Sci.* 92:110–116.
21. Simm, S., J. Einloft, …, E. Schleiff. 2016. 50 years of amino acid hydrophobicity scales: revisiting the capacity for peptide classification. *Biol. Res.* 49:31.
22. Chothia, C. 1976. The nature of the accessible and buried surfaces in proteins. *J. Mol. Biol.* 105:1–12.
23. Acharya, H., S. Vembanur, …, S. Garde. 2010. Mapping hydrophobicity at the nanoscale: applications to heterogeneous surfaces and proteins. *Faraday Discuss.* 146:353–365, discussion 367–393, 395–401.
24. Brusotti, G., E. Calleri, …, C. Temporini. 2018. Advances on size exclusion chromatography and applications on the analysis of protein biopharmaceuticals and protein aggregates: a mini review. *Chromatographia.* 81:3–23.
25. Goyon, A., V. D'Atri, …, D. Guillarme. 2017. Characterization of 30 therapeutic antibodies and related products by size exclusion chromatography: feasibility assessment for future mass spectrometry hyphenation. *J. Chromatogr. B Analyt. Technol. Biomed. Life Sci.* 1065–1066:35–43.
26. Fekete, S., A. Beck, …, D. Guillarme. 2014. Theory and practice of size exclusion chromatography for the analysis of protein aggregates. *J. Pharm. Biomed. Anal.* 101:161–173.
27. Tessier, P. M., A. M. Lenhoff, and S. I. Sandler. 2002. Rapid measurement of protein osmotic second virial coefficients by self-interaction chromatography. *Biophys. J.* 82:1620–1631.
28. Jacobs, S. A., S. J. Wu, …, K. T. O'Neil. 2010. Cross-interaction chromatography: a rapid method to identify highly soluble monoclonal antibody candidates. *Pharm. Res.* 27:65–71.
29. Kohli, N., N. Jain, …, A. A. Lugovskoy. 2015. A novel screening method to assess developability of antibody-like molecules. *MAbs.* 7:752–758.
30. Estep, P., I. Caffry, …, Y. Xu. 2015. An alternative assay to hydrophobic interaction chromatography for high-throughput characterization of monoclonal antibodies. *MAbs.* 7:553–561.
31. Haverick, M., S. Mengisen, …, A. Ambrogelly. 2014. Separation of mAbs molecular variants by analytical hydrophobic interaction chromatography HPLC: overview and applications. *MAbs.* 6:852–858.
32. Jain, T., T. Sun, …, K. D. Wittrup. 2017. Biophysical properties of the clinical-stage antibody landscape. *Proc. Natl. Acad. Sci. USA.* 114:944–949.
33. Black, S. D., and D. R. Mould. 1991. Development of hydrophobicity parameters to analyze proteins which bear post- or cotranslational modifications. *Anal. Biochem.* 193:72–82.
34. Eisenberg, D., E. Schwarz, …, R. Wall. 1984. Analysis of membrane and surface protein sequences with the hydrophobic moment plot. *J. Mol. Biol.* 179:125–142.
35. Zamora, W. J., J. M. Campanera, and F. J. Luque. 2019. Development of a structure-based, pH-dependent lipophilicity scale of amino acids from continuum solvation calculations. *J. Phys. Chem. Lett.* 10:883–889.
36. Bruge, F., S. L. Fornili, …, M. U. Palma. 1996. Solvent-induced forces on a molecular scale: non-additivity, modulation and causal relation to hydration. *Chem. Phys. Lett.* 254:283–291.
37. Wang, L., R. A. Friesner, and B. J. Berne. 2010. Hydrophobic interactions in model enclosures from small to large length scales: non-additivity in explicit and implicit solvent models. *Faraday Discuss.* 146:247–262, discussion 283–298, 395–401.
38. Jamadagni, S. N., R. Godawat, and S. Garde. 2011. Hydrophobicity of proteins and interfaces: insights from density fluctuations. *Annu. Rev. Chem. Biomol. Eng.* 2:147–171.
39. Hummer, G., S. Garde, …, L. R. Pratt. 1996. An information theory model of hydrophobic interactions. *Proc. Natl. Acad. Sci. USA.* 93:8951–8955.

40. Pratt, L. R., M. I. Chaudhari, and S. B. Rempe. 2016. Statistical analyses of hydrophobic interactions: a mini-review. *J. Phys. Chem. B.* 120:6455–6460.

41. Nguyen, C., M. K. Gilson, and T. K. Young. 2011. Structure and thermodynamics of molecular hydration via grid inhomogeneous solvation theory. *arXiv*, arXiv:1108.4876v1 http://arxiv.org/abs/1108.4876v1.

42. Nguyen, C. N., T. K. Young, and M. K. Gilson. 2012. Grid inhomogeneous solvation theory: hydration structure and thermodynamics of the miniature receptor cucurbit[7]uril. *J. Chem. Phys.* 137:044101.

43. Nguyen, C. N., A. Cruz, …, T. Kurtzman. 2014. Thermodynamics of water in an enzyme active site: grid-based hydration analysis of coagulation factor Xa. *J. Chem. Theory Comput.* 10:2769–2780.

44. Ramsey, S., C. Nguyen, …, T. Kurtzman. 2016. Solvation thermodynamic mapping of molecular surfaces in AmberTools: GIST. *J. Comput. Chem.* 37:2029–2037.

45. Kraml, J., A. S. Kamenik, …, K. R. Liedl. 2019. Solvation free energy as a measure of hydrophobicity: application to serine protease binding interfaces. *J. Chem. Theory Comput.* 15:5872–5882.

46. Henzler-Wildman, K., and D. Kern. 2007. Dynamic personalities of proteins. *Nature.* 450:964–972.

47. Boehr, D. D., R. Nussinov, and P. E. Wright. 2009. The role of dynamic conformational ensembles in biomolecular recognition. *Nat. Chem. Biol.* 5:789–796.

48. Jay, J. W., B. Bray, …, G. Ren. 2018. IgG antibody 3D structures and dynamics. *Antibodies (Basel).* 7:18.

49. Blech, M., S. Hörer, …, P. Garidel. 2019. Structure of a therapeutic full-length anti-NPRA IgG4 antibody: dissecting conformational diversity. *Biophys. J.* 116:1637–1649.

50. Fernández-Quintero, M. L., J. Kraml, …, K. R. Liedl. 2019. CDR-H3 loop ensemble in solution - conformational selection upon antibody binding. *MAbs.* 11:1077–1088.

51. Fernández-Quintero, M. L., J. R. Loeffler, …, K. R. Liedl. 2019. Characterizing the diversity of the CDR-H3 loop conformational ensembles in relationship to antibody binding properties. *Front. Immunol.* 9:3065.

52. Fernández-Quintero, M. L., B. A. Math, …, K. R. Liedl. 2019. Transitions of CDR-L3 loop canonical cluster conformations on the micro-to-millisecond timescale. *Front. Immunol.* 10:2652.

53. Fernández-Quintero, M. L., M. C. Heiss, …, K. R. Liedl. 2020. Antibody CDR loops as ensembles in solution vs. canonical clusters from X-ray structures. *MAbs.* 12:1744328.

54. Henderson, R., B. E. Watts, …, S. M. Alam. 2019. Selection of immunoglobulin elbow region mutations impacts interdomain conformational flexibility in HIV-1 broadly neutralizing antibodies. *Nat. Commun.* 10:654.

55. Søndergaard, C. R., M. H. M. Olsson, …, J. H. Jensen. 2011. Improved treatment of ligands and coupling effects in empirical calculation and rationalization of pKa values. *J. Chem. Theory Comput.* 7:2284–2295.

56. Bashford, D., and M. Karplus. 1990. pKa's of ionizable groups in proteins: atomic detail from a continuum electrostatic model. *Biochemistry.* 29:10219–10225.

57. Alexov, E., E. L. Mehler, …, J. M. Word. 2011. Progress in the prediction of pKa values in proteins. *Proteins.* 79:3260–3275.

58. Chen, W., B. H. Morrow, …, J. K. Shen. 2014. Recent development and application of constant pH molecular dynamics. *Mol. Simul.* 40:830–838.

59. Swails, J. M., D. M. York, and A. E. Roitberg. 2014. Constant pH replica exchange molecular dynamics in explicit solvent using discrete protonation states: implementation, testing, and validation. *J. Chem. Theory Comput.* 10:1341–1352.

60. Miao, Y., V. A. Feher, and J. A. McCammon. 2015. Gaussian accelerated molecular dynamics: unconstrained enhanced sampling and free energy calculation. *J. Chem. Theory Comput.* 11:3584–3595.

61. Lazaridis, T. 1998. Inhomogeneous fluid approach to solvation thermodynamics. 1. Theory. *J. Phys. Chem. B.* 102:3531–3541.

62. Loeffler, J. R., M. Schauperl, and K. R. Liedl. 2019. Hydration of aromatic heterocycles as an adversary of π-stacking. *J. Chem. Inf. Model.* 59:4209–4219.

63. Berman, H. M., J. Westbrook, …, P. E. Bourne. 2000. The Protein Data Bank. *Nucleic Acids Res.* 28:235–242.

64. Lyskov, S., F. C. Chou, …, R. Das. 2013. Serverification of molecular modeling applications: the rosetta online server that includes everyone (ROSIE). *PLoS One.* 8:e63906.

65. Marze, N. A., S. Lyskov, and J. J. Gray. 2016. Improved prediction of antibody VL-VH orientation. *Protein Eng. Des. Sel.* 29:409–418.

66. Sivasubramanian, A., A. Sircar, …, J. J. Gray. 2009. Toward high-resolution homology modeling of antibody Fv regions and application to antibody-antigen docking. *Proteins.* 74:497–514.

67. Weitzner, B. D., and J. J. Gray. 2017. Accurate structure prediction of CDR H3 loops enabled by a novel structure-based C-terminal constraint. *J. Immunol.* 198:505–515.

68. Weitzner, B. D., J. R. Jeliazkov, …, J. J. Gray. 2017. Modeling and docking of antibody structures with Rosetta. *Nat. Protoc.* 12:401–416.

69. Stein, A., and T. Kortemme. 2013. Improvements to robotics-inspired conformational sampling in rosetta. *PLoS One.* 8:e63090.

70. Case, D. A., I. Y. Ben-Shalom, …, P. A. Kollman. 2019. AMBER 2019. University of California, San Francisco, CA.

71. Maier, J. A., C. Martinez, …, C. Simmerling. 2015. ff14SB: improving the accuracy of protein side chain and backbone parameters from ff99SB. *J. Chem. Theory Comput.* 11:3696–3713.

72. Jorgensen, W. L., J. Chandrasekhar, …, M. L. Klein. 1983. Comparison of simple potential functions for simulating liquid water. *J. Chem. Phys.* 79:926–935.

73. Darden, T., D. York, and L. Pedersen. 1993. Particle mesh Ewald: an $N\cdot\log(N)$ method for Ewald sums in large systems. *J. Chem. Phys.* 98:10089–10092.

74. Ryckaert, J.-P., G. Ciccotti, and H. J. C. Berendsen. 1977. Numerical integration of the cartesian equations of motion of a system with constraints: molecular dynamics of n-alkanes. *J. Comput. Phys.* 23:327–341.

75. Adelman, S. A., and J. D. Doll. 1976. Generalized Langevin equation approach for atom-solid-surface scattering - general formulation for classical scattering off harmonic solids. *J. Chem. Phys.* 64:2375–2388.

76. Åqvist, J., P. Wennerström, …, B. O. Brandsdal. 2004. Molecular dynamics simulations of water and biomolecules with a Monte Carlo constant pressure algorithm. *Chem. Phys. Lett.* 384:288–294.

77. Berendsen, H. J. C., J. P. M. Postma, …, J. R. Haak. 1984. Molecular-dynamics with coupling to an external bath. *J. Chem. Phys.* 81:3684–3690.

78. Wallnoefer, H. G., S. Handschuh, …, T. Fox. 2010. Stabilizing of a globular protein by a highly complex water network: a molecular dynamics simulation study on factor Xa. *J. Phys. Chem. B.* 114:7405–7412.

79. Case, D. A., I. Y. Ben-Shalom, …, P. A. Kollman. 2018. AMBER 2018. University of California, San Francisco, CA.

80. Shao, J., S. W. Tanner, …, T. E. Cheatham. 2007. Clustering molecular dynamics trajectories: 1. Characterizing the performance of different clustering algorithms. *J. Chem. Theory Comput.* 3:2312–2334.

81. Miao, Y., W. Sinko, …, J. A. McCammon. 2014. Improved reweighting of accelerated molecular dynamics simulations for free energy calculation. *J. Chem. Theory Comput.* 10:2677–2689.

82. Python Software Foundation.. Python language reference, version 3.7. http://www.python.org.

83. Virtanen, P., R. Gommers, …, P. van Mulbregt; SciPy 1.0 Contributors. 2020. SciPy 1.0: fundamental algorithms for scientific computing in Python. *Nat. Methods.* 17:261–272.

84. Dunbar, J., A. Fuchs, …, C. M. Deane. 2013. ABangle: characterising the VH-VL orientation in antibodies. *Protein Eng. Des. Sel.* 26:611–620.

85. Deserno, M. 2004. How to generate equidistributed points on the surface of a sphere https://www.cmu.edu/biolphys/deserno/pdf/sphere_equi.pdf.

86. McInnes, L., J. Healy, and J. Melville. 2018. UMAP: uniform manifold approximation and projection for dimension reduction. *arXiv*, arXiv:1802.03426 https://arxiv.org/abs/1802.03426.

87. Schrodinger, LLC. 2015. The PyMOL molecular graphics system, version 1.8.

88. Hebditch, M., A. Roche, …, J. Warwicker. 2019. Models for antibody behavior in hydrophobic interaction chromatography and in self-association. *J. Pharm. Sci.* 108:1434–1441.

89. van der Kant, R., A. R. Karow-Zwick, …, F. Rousseau. 2017. Prediction and reduction of the aggregation of monoclonal antibodies. *J. Mol. Biol.* 429:1244–1261.

90. Foote, J., and C. Milstein. 1994. Conformational isomerism and the diversity of antibodies. *Proc. Natl. Acad. Sci. USA.* 91:10370–10374.

91. James, L. C., P. Roversi, and D. S. Tawfik. 2003. Antibody multispecificity mediated by conformational diversity. *Science.* 299:1362–1367.

92. Landsteiner, K. 1962. The Specificity of Serological Reactions. Dover Publications, New York.

93. Wedemayer, G. J., P. A. Patten, …, R. C. Stevens. 1997. Structural insights into the evolution of an antibody combining site. *Science.* 276:1665–1669.

94. Pauling, L. 1940. A theory of the structure and process of formation of antibodies. *J. Am. Chem. Soc.* 62:2643–2657.

95. Kossiakoff, A. A., M. Randal, …, C. Eigenbrot. 1992. Variability of conformations at crystal contacts in BPTI represent true low-energy structures: correspondence among lattice packing and molecular dynamics structures. *Proteins.* 14:65–74.

96. Rapp, C. S., and R. M. Pollack. 2005. Crystal packing effects on protein loops. *Proteins.* 60:103–109.

97. Almagro, J. C., A. Teplyakov, …, G. L. Gilliland. 2014. Second antibody modeling assessment (AMA-II). *Proteins.* 82:1553–1562.

98. Schroeder, H. W., Jr., and L. Cavacini. 2010. Structure and function of immunoglobulins. *J. Allergy Clin. Immunol.* 125:S41–S52.

99. Chothia, C., and A. M. Lesk. 1987. Canonical structures for the hypervariable regions of immunoglobulins. *J. Mol. Biol.* 196:901–917.

100. Morea, V., A. Tramontano, …, A. M. Lesk. 1997. Antibody structure, prediction and redesign. *Biophys. Chem.* 68:9–16.

101. Regep, C., G. Georges, …, C. M. Deane. 2017. The H3 loop of antibodies shows unique structural characteristics. *Proteins.* 85:1311–1318.

102. Walsh, I., F. Seno, …, A. Trovato. 2014. PASTA 2.0: an improved server for protein aggregation prediction. *Nucleic Acids Res.* 42:W301–W307.

103. Sormanni, P., F. A. Aprile, and M. Vendruscolo. 2015. The CamSol method of rational design of protein mutants with enhanced solubility. *J. Mol. Biol.* 427:478–490.

104. Schauperl, M., M. Podewitz, …, K. R. Liedl. 2016. Enthalpic and entropic contributions to hydrophobicity. *J. Chem. Theory Comput.* 12:4600–4610.

105. Lauer, T. M., N. J. Agrawal, …, B. L. Trout. 2012. Developability index: a rapid in silico tool for the screening of antibody aggregation propensity. *J. Pharm. Sci.* 101:102–115.

Biophysical Journal, Volume *120*

Supplemental Information

Conformational Ensembles of Antibodies Determine Their Hydrophobicity

Franz Waibl, Monica L. Fernández-Quintero, Anna S. Kamenik, Johannes Kraml, Florian Hofer, Hubert Kettenberger, Guy Georges, and Klaus R. Liedl

Conformational Ensembles of Antibodies Determine Their Hydrophobicity

Effect of Conformation and Protonation

Franz Waibl[1] (FW), Monica L. Fernández-Quintero[1] (MLF), Anna S. Kamenik[1] (ASK), Johannes Kraml[1] (JK), Florian Hofer[1] (FH), Hubert Kettenberger[2] (HK), Guy Georges[2] (GG), Klaus R. Liedl[1*] (KRL)
1: Institute of General, Inorganic and Theoretical Chemistry, and Center for Molecular Biosciences Innsbruck (CMBI), University of Innsbruck, Innsbruck, Austria
2: Roche Pharma Research and Early Development, Large Molecule Research, Roche Innovation Center Munich, Penzberg, Germany

Supporting Information

1. Combining ΔG(solv) of cluster representatives

Given a set of conformations (in this case, cluster representatives), for each of which the free energy of solvation ΔGsolv has been estimated using GIST, the free energy of solvation of the ensemble is given as

$$\Delta G_{solv} = k_B T \ln \int e^{\frac{\Delta G_{solv}(q)}{k_B T}} p(q) dq$$

Where k_B is Boltzmann's constant, T is the temperature, q denotes the cartesian coordinates of the respective conformation, $p(q)$ is the probability of the conformation (or, in the case of cluster representatives, the population of the respective cluster), and $\Delta G_{solv}(q)$ is the hydration free energy of the conformation.
This equation places a high weight on conformations with a positive free energy of hydration. Conceptually, this stems from the fact that ΔG_{solv} is not purely a property of the simulated (solution) state, but a difference between two different states, the reference state being defined by an isolated solute in gas phase and all the water being transferred to the bulk. In the present publication, we estimate cluster probabilities in the liquid state. Since conformations with a high (not very negative) ΔG_{solv} are most favorable in the gas phase, they are the most likely to participate in the equilibrium between solution and gas states, and therefore need to be given a higher weight. If our cluster probabilities had been determined in the gas state, we would need to use a different equation.

We begin our derivation by writing ΔG_{solv} in terms of partition sums:

$$\frac{\Delta G_{solv}}{k_B T} = -\ln \frac{Z^{sol}}{Z^u Z^v} = \ln \frac{Z^u Z^v}{Z^{sol}} \quad (1)$$

Where Z^{sol}, Z^v, and Z^u represent the partition sums of the solution, the pure solvent, and the solute in gas phase, respectively.

Writing out the terms of the partition sums gives:

$$Z^u = \int e^{-\frac{H^{uu}(q_u)}{k_B T}} dq_u \quad (2)$$

$$Z^v = \int e^{-\frac{H^{vv}(q_v)}{k_B T}} dq_v \quad (3)$$

$$Z^{sol} = \int\int e^{-\frac{H^{uu}(q_u)+H^{vv}(q_v)+H^{uv}(q_u,q_v)}{k_B T}} dq_v dq_u \quad (4)$$

Where q_u denotes the solute degrees of freedom, qv the solvent degrees of freedom, and H^{uu}, H^{vv}, and H^{uv} denote the solute-solute, solvent-solvent, and solute-solvent energy contributions.

The probability of finding a solute conformation $p(q_u)$ in a molecular dynamics simulation is:

$$p(q_u) = \frac{\int e^{-\frac{H^{uu}(q_u)+H^{vv}(q_v)+H^{uv}(q_u,q_v)}{k_B T}} dq_v}{Z^{sol}} \quad (5)$$

Assuming that H^{uu} is independent of the solvent degrees of freedom, we write this as:

$$p(q_u) = \frac{\int e^{-\frac{H^{vv}(q_v)+H^{uv}(q_u,q_v)}{k_B T}} dq_v \, e^{-\frac{H^{uu}(q_u)}{k_B T}}}{Z^{sol}} \quad (6)$$

From each GIST calculation, we obtain an estimate of the hydration free energy of a single solute conformation, i.e., the change in free energy upon placing a solute *in this conformation* from the gas phase into the solution phase. We write this as:

$$e^{-\frac{\Delta G_{solv}(q_u)}{k_B T}} = \frac{\int e^{-\frac{H^{vv}(q_v)+H^{uv}(q_u,q_v)}{k_B T}} dq_v}{Z^v} \quad (7)$$

Here, the partition sum of the solute Z^v is practically introduced by referencing our GIST results to a pure solvent box.

Inserting the righthand side of Eq. 7 into Eq. 6 gives us:

$$p(q_u) = \frac{e^{-\frac{\Delta G_{solv}(q_u)}{k_B T}} e^{-\frac{H^{uu}(q_u)}{k_B T}} Z^v}{Z^{sol}} \quad (8)$$

To arrive at an expression of the total ΔGsolv, we first note that we do not have an expression for the (gas phase) solute ensemble Zu. We therefore seek to express Eq. 2 in terms of other quantities. We do so by separating the term involving Huu in Eq. 8 and inserting it to Eq. 2. We arrive at:

$$Z^u = \frac{\int p(q_u) e^{\frac{\Delta G_{solv}(q_u)}{k_B T}} Z^{sol}}{Z^v} dq_u \quad (9)$$

Note the positive sign before $\Delta G_{solv}(q_u)$ that arises from taking its reciprocal value. Z^u and Z^{sol} are already integrals and therefore independent of q_u and can be separated.

Inserting Eq. 9 in Eq. 1 results in:

$$\frac{\Delta G_{solv}}{k_B T} = \ln \int p(q_u) e^{\frac{\Delta G_{solv}(q_u)}{k_B T}} dq_u \quad (10)$$

2. Used PDB codes

SI Table 1: PDB codes used as starting structures for the molecular dynamics (both GaMD and CpHMD) simulations.

Antibody	PDB
Adalimumab	4NYL
alemtuzumab	1BEY
Anifrolumab	4QXG
Atezolizumab	5X8L
bapineuzumab	4OJF
Basiliximab	1MIM
Belimumab	5Y9J
Bevacizumab	1BJ1
Bevacizumab	6BFT
Bimagrumab	5NGV
Briakinumab	5N2K
Canakinumab	4G6J
Certolizumab	5WUX
Cetuximab	1YY8
Crenezumab	5VZY
Daclizumab	3NFP
Drozitumab	4OD2
Eculizumab	5I5K
Efalizumab	3EOA
epratuzumab	5VL3
gantenerumab	5CSZ
gevokizumab	4G6M
Golimumab	5YOY
Ibalizumab	3O2D
Infliximab	4G3Y
Ipilimumab	5TRU
ixekizumab	6NOV
lebrikizumab	4I77
matuzumab	3C09
motavizumab	3IXT
muromonab	1SY6
natalizumab	4IRZ
necitumumab	6B3S
nivolumab	5WT9
ofatumumab	3GIZ
olokizumab	4CNI
omalizumab	2XA8
onartuzumab	4K3J
panitumumab	5SX5
pembrolizumab	5GGS
pertuzumab	1S78
pinatuzumab	6AND
ponezumab	3U0T
ranibizumab	1CZ8
rituximab	6VJA
sifalimumab	4YPG
tanezumab	4EDW
tralokinumab	5L6Y
trastuzumab	1N8Z
tremelimumab	5GGV
urelumab	6MHR
ustekinumab	3HMW

3. Experimental details

In the present work, we use experimental data from a dataset by Jain et al. (1) Here, we shortly describe the experimental conditions of the assays that we mention in the main text. For more detailed information, the reader is referred to the original works.

Hydrophobic Interaction Chromatography:
The methodology described in reference (2) was used. 5 µg (1 mg/mL) of sample was analyzed using a Sepax Proteomix HIC butyl-NP5 column over 20 min. A linear gradient from mobile phase A (1.8M ammonium sulfate and 0.1M sodium phosphate at pH 6.5) to mobile phase B (0.1 M sodium phosphate at pH 6.5) was employed with a flow rate of 1 mL/min. The UV adsorbance was monitored at 280 nm.

Standup Monolayer Adsorption Chromatography:
The methodology described in reference (3) was used. 2 µg of sample was analyzed using a Zenix SEC-300 column. A 0.15M sodium phosphate buffer at pH 7.0 was used as mobile phase, with a flow rate of 0.35 mL/min.

Cross Interaction Chromatography:
The methodology described in reference (4) was used. 5 µg of sample was analyzed using a 1-mL HiTrap column with ~30mg of human serum polyclonal antibodies coupled to it. A PBS buffer was used as mobile phase, with a flow rate of 0.1 mL/min.

4. Effect of the ROC cutoff and the cutoff for $\Delta G_{unfavorable}$

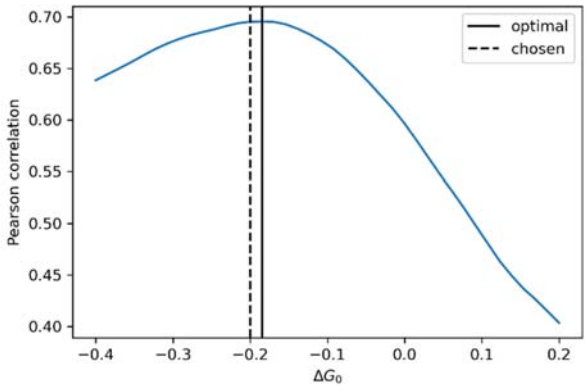

Figure 1: Pearson correlation between experimental HIC retention times of the PDB set and $\Delta G_{unfavorable}$, depending on the x offset in the cutoff function (corresponds to ΔG_0 in Equation 8).The optimal value (the x position with the highest correlation), as well as the rounded value used in this study, are shown as vertical lines. The input data was the ΔG_{solv} values obtained after GaMD sampling of the PDB set. Computing $\Delta G_{unfavorable}$ using the chosen ΔG_0 leads to the data shown in Figure 1E.

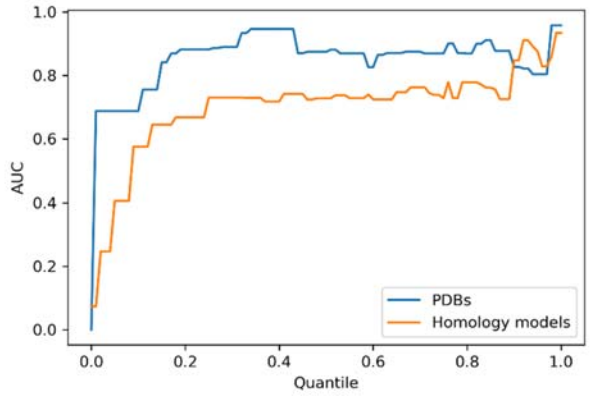

Figure 2: AUC value for the separation between strongly-binding and weakly-binding antibodies in the PDB set (blue) and in the homology models set (orange), depending on the quantile at which the border between strongly-binding and weakly-binding was drawn. The separation was performed based on the $\Delta G_{unfavorable}$ values shown in Figure 1E.

1. Jain, T., T. Sun, S. Durand, A. Hall, N. Houston, J. Nett, B. Sharkey, B. Bobrowicz, I. Caffry, Y. Yu, Y. Cao, H. Lynaugh, M. Brown, H. Baruah, L. Gray, E. Krauland, Y. Xu, M. Vasquez, and K. Wittrup. 2017. Biophysical properties of the clinical-stage antibody landscape. Proceedings of the National Academy of Sciences of the United States of America 114(5):944-949. Article.

2. Estep, P., I. Caffry, Y. Yu, T. W. Sun, Y. Cao, H. Lynaugh, T. Jain, M. Vasquez, P. M. Tessier, and Y. D. Xu. 2015. An alternative assay to hydrophobic interaction chromatography for high-throughput characterization of monoclonal antibodies. Mabs 7(3):553-561.

3. Kohli, N., N. Jain, M. L. Geddie, M. Razlog, L. H. Xu, and A. A. Lugovskoy. 2015. A novel screening method to assess developability of antibody-like molecules. Mabs 7(4):752-758.

4. Jacobs, S. A., S. J. Wu, Y. Q. Feng, D. Bethea, and K. T. O'Neil. 2010. Cross-Interaction Chromatography: A Rapid Method to Identify Highly Soluble Monoclonal Antibody Candidates. Pharm Res-Dordr 27(1):65-71.